Intravital fluorescence imaging of mouse brain using implantable semiconductor devices and epi-illumination of biological tissue

Hiroaki Takehara,[1,2,*] Yasumi Ohta,[2] Mayumi Motoyama,[2] Makito Haruta,[2] Mizuki Nagasaki,[2] Hironari Takehara,[2] Toshihiko Noda,[2] Kiyotaka Sasagawa,[2] Takashi Tokuda,[2] and Jun Ohta[1,2]

[1]*Institute for Research Initiatives, Nara Institute of Science and Technology, 8916-5 Takayama-cho, Ikoma, Nara 630-0192, Japan*

[2]*Graduate School of Materials Science, Nara Institute of Science and Technology, 8916-5 Takayama-cho, Ikoma, Nara 630-0192, Japan*

[*]*takehara@ms.naist.ac.jp*

Abstract: The application of the fluorescence imaging method to living animals, together with the use of genetically engineered animals and synthesized photo-responsive compounds, is a powerful method for investigating brain functions. Here, we report a fluorescence imaging method for the brain surface and deep brain tissue that uses compact and mass-producible semiconductor imaging devices based on complementary metal-oxide semiconductor (CMOS) technology. An image sensor chip was designed to be inserted into brain tissue, and its size was 1500 × 450 μm. Sample illumination is also a key issue for intravital fluorescence imaging. Hence, for the uniform illumination of the imaging area, we propose a new method involving the epi-illumination of living biological tissues, and we performed investigations using optical simulations and experimental evaluation.

OCIS codes: (110.2970) Image detection systems; (170.2655) Functional monitoring and imaging; (280.1415) Biological sensing and sensors.

References and links

1. M. J. Pittet and R. Weissleder, "Intravital imaging," Cell **147**(5), 983–991 (2011).
2. W. R. Zipfel, R. M. Williams, and W. W. Webb, "Nonlinear magic: multiphoton microscopy in the biosciences," Nat. Biotechnol. **21**(11), 1369–1377 (2003).
3. F. Helmchen and W. Denk, "Deep tissue two-photon microscopy," Nat. Methods **2**(12), 932–940 (2005).
4. M. Mank, A. F. Santos, S. Direnberger, T. D. Mrsic-Flogel, S. B. Hofer, V. Stein, T. Hendel, D. F. Reiff, C. Levelt, A. Borst, T. Bonhoeffer, M. Hübener, and O. Griesbeck, "A genetically encoded calcium indicator for chronic *in vivo* two-photon imaging," Nat. Methods **5**(9), 805–811 (2008).
5. D. J. Wallace, S. Meyer zum Alten Borgloh, S. Astori, Y. Yang, M. Bausen, S. Kügler, A. E. Palmer, R. Y. Tsien, R. Sprengel, J. N. Kerr, W. Denk, and M. T. Hasan, "Single-spike detection in vitro and *in vivo* with a genetic Ca2+ sensor," Nat. Methods **5**(9), 797–804 (2008).
6. F. Zhang, A. M. Aravanis, A. Adamantidis, L. de Lecea, and K. Deisseroth, "Circuit-breakers: optical technologies for probing neural signals and systems," Nat. Rev. Neurosci. **8**(8), 577–581 (2007).
7. K. Ohki, S. Chung, Y. H. Ch'ng, P. Kara, and R. C. Reid, "Functional imaging with cellular resolution reveals precise micro-architecture in visual cortex," Nature **433**(7026), 597–603 (2005).
8. M. Matsuzaki, G. C. R. Ellis-Davies, T. Nemoto, Y. Miyashita, M. Iino, and H. Kasai, "Dendritic spine geometry is critical for AMPA receptor expression in hippocampal CA1 pyramidal neurons," Nat. Neurosci. **4**(11), 1086–1092 (2001).
9. J. Noguchi, A. Nagaoka, S. Watanabe, G. C. R. Ellis-Davies, K. Kitamura, M. Kano, M. Matsuzaki, and H. Kasai, "*In vivo* two-photon uncaging of glutamate revealing the structure-function relationships of dendritic spines in the neocortex of adult mice," J. Physiol. **589**(10), 2447–2457 (2011).
10. H. Takehara, A. Nagaoka, J. Noguchi, T. Akagi, H. Kasai, and T. Ichiki, "Lab-on-a-brain: Implantable micro-optical fluidic devices for neural cell analysis *in vivo*," Sci. Rep. **4**, 6721 (2014).

#235764 - $15.00 USD Received 6 Mar 2015; accepted 16 Mar 2015; published 2 Apr 2015
(C) 2015 OSA 1 May 2015 | Vol. 6, No. 5 | DOI:10.1364/BOE.6.001553 | BIOMEDICAL OPTICS EXPRESS 1553

11. R. P. Barretto, T. H. Ko, J. C. Jung, T. J. Wang, G. Capps, A. C. Waters, Y. Ziv, A. Attardo, L. Recht, and M. J. Schnitzer, “Time-lapse imaging of disease progression in deep brain areas using fluorescence microendoscopy,” Nat. Med. **17**(2), 223–228 (2011).
12. P. Kim, E. Chung, H. Yamashita, K. E. Hung, A. Mizoguchi, R. Kucherlapati, D. Fukumura, R. K. Jain, and S. H. Yun, “*In vivo* wide-area cellular imaging by side-view endomicroscopy,” Nat. Methods **7**(4), 303–305 (2010).
13. B. A. Flusberg, E. D. Cocker, W. Piyawattanametha, J. C. Jung, E. L. Cheung, and M. J. Schnitzer, “Fiber-optic fluorescence imaging,” Nat. Methods **2**(12), 941–950 (2005).
14. B. A. Flusberg, A. Nimmerjahn, E. D. Cocker, E. A. Mukamel, R. P. Barretto, T. H. Ko, L. D. Burns, J. C. Jung, and M. J. Schnitzer, “High-speed, miniaturized fluorescence microscopy in freely moving mice,” Nat. Methods **5**(11), 935–938 (2008).
15. K. K. Ghosh, L. D. Burns, E. D. Cocker, A. Nimmerjahn, Y. Ziv, A. E. Gamal, and M. J. Schnitzer, “Miniaturized integration of a fluorescence microscope,” Nat. Methods **8**(10), 871–878 (2011).
16. J. Ohta, T. Tokuda, K. Sasagawa, and T. Noda, “Implantable CMOS biomedical devices,” Sensors (Basel) **9**(11), 9073–9093 (2009).
17. M. Haruta, C. Kitsumoto, Y. Sunaga, H. Takehara, T. Noda, K. Sasagawa, T. Tokuda, and J. Ohta, “An implantable CMOS device for blood-flow imaging during experiments on freely moving rats,” Jpn. J. Appl. Phys. **53**(4S), 04EL05 (2014).
18. A. Tagawa, H. Minami, M. Mitani, T. Noda, K. Sasagawa, T. Tokuda, H. Tamura, Y. Hatanaka, Y. Ishikawa, S. Shiosaka, and J. Ohta, “Multimodal Complementary Metal–Oxide–Semiconductor Sensor Device for Imaging of Fluorescence and Electrical Potential in Deep Brain of Mouse,” Jpn. J. Appl. Phys. **49**(1), 01AG02 (2010).
19. A. Tagawa, M. Mitani, H. Minami, T. Noda, K. Sasagawa, T. Tokuda, and J. Ohta, “Complementary Metal Oxide Semiconductor Based Multimodal Sensor for In vivo Brain Function Imaging with a Function for Simultaneous Cell Stimulation,” Jpn. J. Appl. Phys. **49**, 04DL02 (2010).
20. L. G. Henyey and J. L. Greenstein, “Diffuse radiation in the galaxy,” Astrophys. J. **93**, 70–83 (1941).
21. T. Binzoni, T. Leung, A. Gandjbakhche, D. Rüfenacht, and D. Delpy, “The use of the Henyey–Greenstein phase function in Monte Carlo simulations in biomedical optics,” Phys. Med. Biol. **51**, N313 (2006).
22. G. Hall, S. L. Jacques, K. W. Eliceiri, and P. J. Campagnola, “Goniometric measurements of thick tissue using Monte Carlo simulations to obtain the single scattering anisotropy coefficient,” Biomed. Opt. Express **3**(11), 2707–2719 (2012).
23. J. G. Bernstein, X. Han, M. A. Henninger, E. Y. Ko, X. Qian, G. T. Franzesi, J. P. McConnell, P. Stern, R. Desimone, and E. S. Boyden, “Prosthetic systems for therapeutic optical activation and silencing of genetically-targeted neurons,” Proc. Soc. Photo Opt. Instrum. Eng. **6854**, 68540H (2008).
24. Q. T. Le, A. Ohashi, S. Hirose, and N. Katunuma, “Reverse zymography using fluorogenic substrates for protease inhibitor detection,” Electrophoresis **26**(6), 1038–1045 (2005).
25. D. C. Ng, T. Tokuda, A. Yamamoto, M. Matsuo, M. Nunoshita, H. Tamura, Y. Ishikawa, S. Shiosaka, and J. Ohta, “On-chip biofluorescence imaging inside a brain tissue phantom using a CMOS image sensor for *in vivo* brain imaging verification,” Sens. Actuators B Chem. **119**(1), 262–274 (2006).
26. O. Yizhar, L. E. Fenno, T. J. Davidson, M. Mogri, and K. Deisseroth, “Optogenetics in neural systems,” Neuron **71**(1), 9–34 (2011).
27. O. Barajas, Å. M. Ballangrud, G. G. Miller, R. B. Moore, and J. Tulip, “Monte Carlo modelling of angular radiance in tissue phantoms and human prostate: PDT light dosimetry,” Phys. Med. Biol. **42**(9), 1675–1687 (1997).
28. R. M. Valentine, K. Wood, C. T. Brown, S. H. Ibbotson, and H. Moseley, “Monte Carlo simulations for optimal light delivery in photodynamic therapy of non-melanoma skin cancer,” Phys. Med. Biol. **57**(20), 6327–6345 (2012).
29. A. M. Aravanis, L. P. Wang, F. Zhang, L. A. Meltzer, M. Z. Mogri, M. B. Schneider, and K. Deisseroth, “An optical neural interface: *in vivo* control of rodent motor cortex with integrated fiberoptic and optogenetic technology,” J. Neural Eng. **4**(3), S143–S156 (2007).
30. D. Huber, L. Petreanu, N. Ghitani, S. Ranade, T. Hromádka, Z. Mainen, and K. Svoboda, “Sparse optical microstimulation in barrel cortex drives learned behaviour in freely moving mice,” Nature **451**(7174), 61–64 (2008).
31. A. Koehler, “New method of illumination for phomicrographical purposes,” J. Roy. Microscop. Soc. **14**, 261–262 (1894).
32. P. Ruffieux, T. Scharf, I. Philipoussis, H. P. Herzig, R. Voelkel, and K. J. Weible, “Two step process for the fabrication of diffraction limited concave microlens arrays,” Opt. Express **16**(24), 19541–19549 (2008).
33. C. Y. Wu, T. H. Chiang, and C. C. Hsu, “Fabrication of microlens array diffuser films with controllable haze distribution by combination of breath figures and replica molding methods,” Opt. Express **16**(24), 19978–19986 (2008).
34. D. Sakai, K. Harada, S. Kamemaru, M. A. El-Morsy, M. Itoh, and T. Yatagai, “Direct fabrication of surface relief holographic diffusers in azobenzene polymer films,” Opt. Rev. **12**(5), 383–386 (2005).
35. J.-H. Wang, S.-Y. Lien, J.-R. Ho, T.-K. Shih, C.-F. Chen, C.-C. Chen, and W.-T. Whang, “Optical diffusers based on silicone emulsions,” Opt. Mater. **32**(2), 374–377 (2009).
36. G. Kim, “A PMMA composite as an optical diffuser in a liquid crystal display backlighting unit (BLU),” Eur. Polym. J. **41**(8), 1729–1737 (2005).

#235764 - $15.00 USD Received 6 Mar 2015; accepted 16 Mar 2015; published 2 Apr 2015

37. H. Tamura, D. C. Ng, T. Tokuda, H. Naoki, T. Nakagawa, T. Mizuno, Y. Hatanaka, Y. Ishikawa, J. Ohta, and S. Shiosaka, “One-chip sensing device (biomedical photonic LSI) enabled to assess hippocampal steep and gradual up-regulated proteolytic activities,” J. Neurosci. Methods **173**(1), 114–120 (2008).
38. M. Choi, J. W. Choi, S. Kim, S. Nizamoglu, S. K. Hahn, and S. H. Yun, “Light-guiding hydrogels for cell-based sensing and optogenetic synthesis in vivo,” Nat. Photonics **7**(12), 987–994 (2013).
39. E. Petryayeva, W. R. Algar, and I. L. Medintz, “Quantum dots in bioanalysis: a review of applications across various platforms for fluorescence spectroscopy and imaging,” Appl. Spectrosc. **67**(3), 215–252 (2013).
40. X. Michalet, F. F. Pinaud, L. A. Bentolila, J. M. Tsay, S. Doose, J. J. Li, G. Sundaresan, A. M. Wu, S. S. Gambhir, and S. Weiss, “Quantum dots for live cells, in vivo imaging, and diagnostics,” Science **307**(5709), 538–544 (2005).
41. R. G. Aswathy, Y. Yoshida, T. Maekawa, and D. S. Kumar, “Near-infrared quantum dots for deep tissue imaging,” Anal. Bioanal. Chem. **397**(4), 1417–1435 (2010).
42. P. A. Mayes, D. T. Dicker, Y. Y. Liu, and W. S. El-Deiry, “Noninvasive vascular imaging in fluorescent tumors using multispectral unmixing,” Biotechniques **45**(4), 459–464 (2008).
43. S. Sekiya, T. Shimizu, and T. Okano, “Vascularization in 3D tissue using cell sheet technology,” Regen. Med. **8**(3), 371–377 (2013).
44. H. Takehara, K. Miyazawa, T. Noda, K. Sasagawa, T. Tokuda, S. H. Kim, R. Iino, H. Noji, and J. Ohta, “A CMOS image sensor with low fixed pattern noise suitable for lensless observation system of digital enzyme-linked immunosorbent assay (ELISA),” *in Proceedings of IEEE Conference on International Meeting for Future of Electron Devices, Kansai (IMFEDK, 2013)*, 32–33.

1. Introduction

Recent advances in intravital imaging techniques for the investigation of neural networks in living animals have led to new insights into the brain [1–3]. Neural cells and biochemical reactions in an intact brain can be optically identified and controlled using genetically engineered mice [4–6] and synthesized photo-responsive compounds [7–10]. Although intravital fluorescence imaging has already shown great potential as a powerful tool in neuroscience, several technical issues remain. For example, the imaging area is limited (<1 mm in depth) owing to light absorption and scattering in biological tissues and immobilization under the objective lens of tabletop-type microscopes prevents imaging in freely behaving animals.

Therefore, extensive efforts have been devoted to overcoming those limitations, and several techniques using gradient refractive index (GRIN) lens [11,12] and optical fiber bundles [13,14], have been developed. Those optical elements were implanted into a certain part of the skull bone and connected to the objective lens of tabletop-type microscopes to obtain fluorescent images. Ghosh *et al.* reported a fully miniaturized optical microscope, with a series of lenses, a focusing mechanical structure and an image sensor, and these enabled the observation of the microvascular network in living mice [15].

Complementary metal-oxide semiconductor (CMOS) technology enables simple and compact imaging devices for intravital imaging [16–19]. Imaging devices based on CMOS technology have the following important advantages: (1) Simple device design without optical elements, such as objective lens and relay lens, is mass-producible and feasible for disposable use. (2) A compact size of several hundred micrometers means low invasiveness to animals and feasibility for long-term imaging even under freely moving conditions. (3) CMOS technology enables the integration of image data acquisition, compression, logging, analysis, electrical measurement [18], and stimulation [19] on a single chip, and the large-scale integration based on CMOS technology is highly attractive for *in situ* monitoring and diagnostics of brain diseases as medical applications (e.g. wireless communication, deep brain stimulation, and the brain machine-interface).

In this paper, we propose a fluorescence imaging method for the brain surfaces and deep brain tissue using a combination of implantable micro-semiconductor imaging devices and epi-illumination of biological tissues. We describe the device design, fabrication process, and performance evaluation. For the uniform illumination of tissues in the imaging area, we studied the epi-illumination method using the optical simulation of a brain tissue model. To demonstrate intravital fluorescence imaging, we imaged fluorescent microspheres and blood vessels labeled with quantum dots using the developed devices.

2. Methods

All experimental protocols were approved by the Animal Experiment Committee of Nara Institute of Science and Technology, and all animal care and experimental procedures were carried out in accordance with the Guidelines for the Care and Use of Laboratory Animals of the Nara Institute of Science and Technology.

2.1 Schematics of intravital fluorescence imaging of brain tissue

Figure 1 shows the schematics of intravital fluorescence imaging using a combination of an implantable semiconductor imaging device and the epi-illumination method for brain tissue. The device was implanted into a certain part of the brain tissue and an epi-illumination light source was placed on the surface of the brain. Scattered light illuminated the brain tissue for fluorescence imaging. Fluorescent images can be obtained with an implanted image sensor.

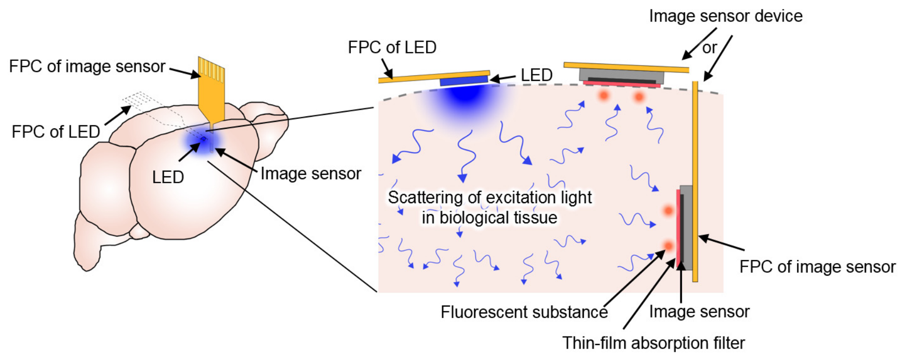

Fig. 1. Schematics of epi-illumination and imaging in brain tissues using a light-emitting diode (LED) and a semiconductor imaging device.

2.2 Device design

Figures 2(a) and 2(b) show a schematic and a photograph of the implantable semiconductor imaging device. As shown in Fig. 2(a), the structure comprises three parts: a CMOS image-sensor chip, an absorption filter layer and a flexible printed circuit (FPC). The absorption filter is directly coated onto the image sensor. Passage through the absorption filter ensures that only fluorescent light can be detected by the image sensor. The CMOS image-sensor chip was connected to a personal computer (PC) via the FPC, a small relay board, and a control board, and was controlled by software as previously reported in detail in [17,18].

2.3 Device fabrication

The fabrication process of the implantable semiconductor imaging device is shown in Fig. 2(c), and is described as follows. First, the CMOS image-sensor chip with a width of 450 μm, length of 1500 μm, and thickness of 150 μm was fixed onto the FPC using epoxy resin (EPO-TEK 730, Epoxy Technology Inc., Billerica, MA, USA) by heating at 120°C for 15 min. Second, four bonding pads of the CMOS image-sensor chip were connected to the FPC via Al wires using a wire bonder (7700CP, West Bond Inc., Anaheim, CA, USA). Third, an absorption filter (SR-3000L, Fujifilm Electronic Materials Co., Ltd, Japan) was spin-coated, covering the image sensor area. Finally, the implantable semiconductor imaging device was coated with a 2-μm thick layer of parylene film for waterproofing.

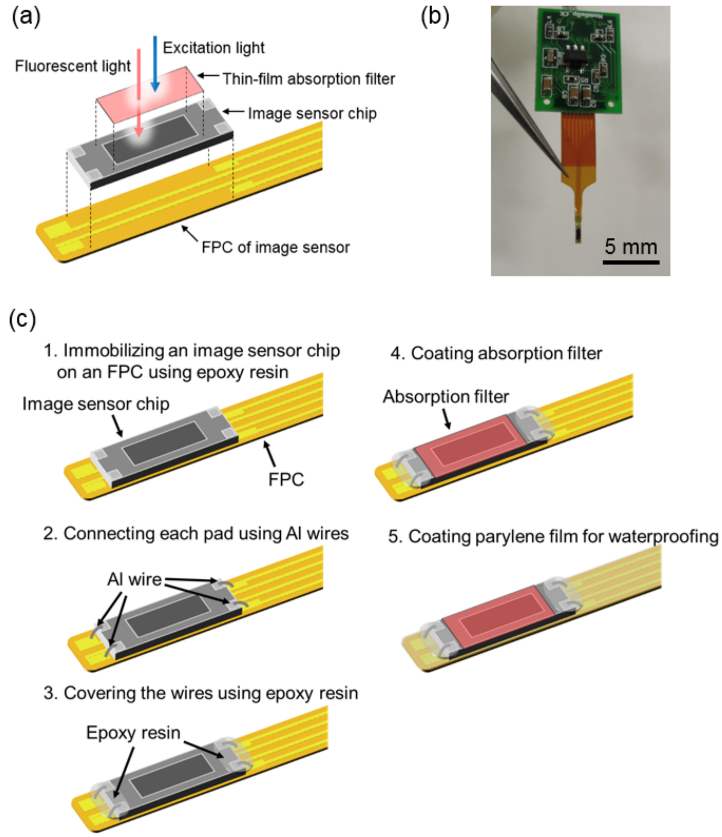

Fig. 2. Schematics and photographs of the implantable semiconductor imaging device. (a) Schematics of the implantable semiconductor imaging device. The device is constructed with a thin-film absorption filter, an imaging sensor chip, and a flexible printed circuit (FPC). (b) Photograph of the implantable semiconductor imaging device. The semiconductor image sensor chip is immobilized onto the FPC, which is connected to the small relay board. (c) Fabrication process of the implantable semiconductor imaging device.

2.4 CMOS image-sensor chip

Figure 3(a) and Table 1 show a photograph and the specifications of the CMOS image-sensor chip, respectively. The image sensor was designed to be controlled by four wires (V_{DD}, GND, CLK, and Out), as shown in Fig. 3(b). The sensor chip was fabricated by a 0.35-µm 2-poly 4-metal standard CMOS technology. The linearity of output signal of the image sensor as a function of light intensity is shown in Fig. 3(c), and only the linear region was used in evaluation experiments of light intensity distribution in brain tissues.

Table 1. Specifications of fabricated CMOS image-sensor chip

Process technology	0.35-µm 2-poly 4-metal standard CMOS process
Supply voltage (V)	3.3
Chip size (μm^2)	450 × 1500
Pixel type	3-transistor active pixel sensor
Pixel size (μm^2)	7.5 × 7.5
Pixel array size	40 × 120
Photodiode type	N-well–P-sub.
Fill factor (%)	44

#235764 - $15.00 USD Received 6 Mar 2015; accepted 16 Mar 2015; published 2 Apr 2015

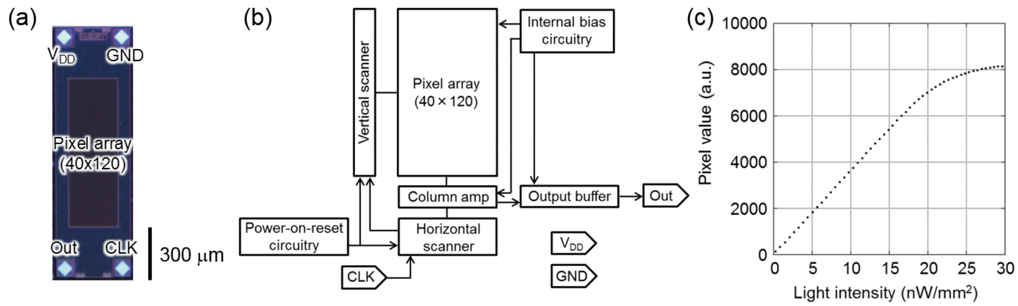

Fig. 3. Schematics and photographs of fabricated CMOS image-sensor chip. (a) The CMOS imaging-sensor chip has a pixel array and four bonding pads. The imaging sensor chip is 450-μm wide, 1500-μm long, and 150-μm thick. (b) Block diagram of the CMOS image-sensor chip. The chip has three inputs (V_{DD}, GND, and CLK) and one output (Out). Schematics of output circuit was reported in detail elsewhere [44]. (c) Sensitivity of the CMOS image-sensor chip.

2.5 Evaluation of absorption filters

To evaluate the absorption filter performance, we varied the film thickness from 0.8 to 3.4 μm. For each thickness, the transmittance at $\lambda = 470$ nm was measured using an optical power meter (S120VC and PM100USB, Thorlabs Inc., Newton, NJ, USA). The spectral transmittance was measured using spectral apparatus (MCPD-3700, Otsuka Electronics Co., Ltd., Osaka, Japan). To verify the resolution of the image sensor integrated with the absorption filter, the full width at half maximum (FWHM) was measured with red fluorescent microspheres of 15-μm diameter (F21012, Life technologies Inc., Grand Island, NY, USA) on the surface of the device. The excitation peak of the microsphere was 565 nm and the emission peak was 580 nm.

2.6 Epi-illumination method of brain tissues

For minimum invasiveness to animals, an inexpensive and compact blue-light-emitting diode (LED) of 280-μm width, 305-μm height, and 90-μm thickness (ES-CEBHM12A, Epistar Corp., Taiwan) was used as an epi-illumination light source for brain tissue. The supply of current to the LED was controlled by a programmable dc power supply (R6144, Advantest Corp., Tokyo, Japan). To avoid heat damage to the brain tissue, the dc power was set in the range 0.2–1.4 mA. The output power of the LED was measured with the optical power meter. The monitored optical power was in the range 0.2–1.1 mW mm^{-2}.

2.7 Optical simulation

To evaluate the optical power distribution in the brain tissue, we performed a numerical simulation using a commercially available software package (FRED, Photon Engineering, LLC, AZ, USA). A brain tissue model was set as an anisotropic model based on the Henyey–Greenstein phase function [20–22]. Photons in a Lambertian radiation pattern from the surface of the LED were launched and traced in the brain tissue model. Simulations were conducted using appropriate optical parameters of brain tissues (absorption coefficient $\mu_a = 0.07$ mm^{-1}, scattering coefficient $\mu_s = 10$ mm^{-1}, Henyey–Greenstein phase function g = 0.88) [23].

2.8 Surgical implantation

Implantation experiments were performed as follows. An adult mouse (C57BL6) was initially anesthetized by injecting urethane. The skull (1.0-mm posterior, 1.3-mm lateral to bregma) was partially removed using a dental drill. After the removal of the skull bone, the exposed dura mater was carefully removed. Then, the implantable semiconductor imaging device was inserted into the brain tissue at a depth of 2 mm, and the LED for epi-illumination of the brain tissue was placed at the surface of the brain tissue using a stereotaxis apparatus (SR-5M, Narishige Co., Ltd., Tokyo, Japan).

2.9 Intravital fluorescence imaging in deep brain tissue

Intravital imaging experiments were performed as follows. The mouse was anesthetized and immobilized using the stereotaxis apparatus. The brain tissue was illuminated by the LED and the red fluorescent microspheres of 15-μm diameter mimicking fluorescent cells were placed on the surface of the device and imaged with the image sensor. The distance between the position of the sensor and the LED, L, varied within the range 0–2 mm. The positions of the sensor and the LED were precisely controlled with 50-μm precision using the stereotaxis apparatus, which has three perpendicular shafts for three-dimensional manipulation.

2.10 Fluorescence imaging of fluorescent substance embedded in brain-tissue slice

We prepared 50-μm-thick brain-tissue slices from adult mice (C57BL6). The fluorescent microspheres were embedded into the brain slice. The brain slice was directly placed onto the surface of the image sensor and the microspheres embedded in the brain slice were imaged with the image sensor.

2.11 Intravital fluorescence imaging of blood vessels

Blood vessels were labeled by tail-vein injection of quantum dots. The 100-μL solution of 0.4-μM quantum dots (Q21071MP, Qtracker 800 Vascular Labels, Life Technologies Inc., Grand Island, NY, USA) in physiological saline (Otsuka Pharmaceutical Factory, Inc., Japan) was injected intravenously via the lateral tail vein. The device and the LED were placed onto the surface of the brain, and blood vessels embedded in the brain tissue were imaged with the image sensor.

3. Results

3.1 Characterization of the image sensor with absorption filters

The thickness of absorption filter may cause degradation of the fluorescent image resolution due to light spreading in the filter layer. Thus, the absorption filter for an implantable image sensor requires both (i) sufficient absorption of excitation light (transmittance; $T < 10^{-5}$) and (ii) low thickness (<5 μm) of the filter layer to avoid degradation of the resolution.

Figure 4(a) shows the transmittance at $\lambda = 470$ nm for each thickness. The filter thickness of 3.4 μm produced a transmittance of less than 10^{-5}, which is acceptable excitation light absorption performance. The transmittance spectrum of the 3.4-μm thick filter was measured as shown in Fig. 4(b), and a sharp change in transmittance that allows sufficient separation of the fluorescent signal from the excitation light was observed at approximately 570 nm.

Subsequently, a fluorescence imaging test was performed using the semiconductor imaging device integrated with the thin-film absorption filter. Figure 4(c) shows a fluorescent image obtained by the image sensor that was integrated with the 3.4-μm thick absorption filter. Fluorescent microspheres ($\phi = 15$ μm) were clearly observed, and the full width at half maximum (FWHM) was evaluated as 22.3 ± 0.5 μm. Considering that size of the image sensor pixels was 7.5×7.5 μm, the film thickness of the absorption filter did not degrade the image resolution. The resolution of the developed device can be used in the study of brain activities using genetically engineered animals [4,5] and fluorogenic substrates [24,25].

#235764 - $15.00 USD Received 6 Mar 2015; accepted 16 Mar 2015; published 2 Apr 2015

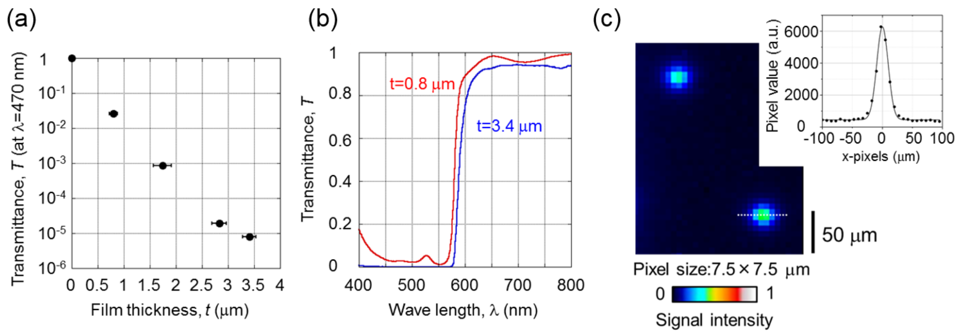

Fig. 4. Performance of thin-film absorption filters and the semiconductor imaging device integrated with the thin-film absorption filter. (a) Transmittance T at 470 nm as a function of film thickness t (μm) of the absorption filter. The film thickness was controlled by the numbers of spin-coated layers. Horizontal error bars show the standard deviations of the thickness. (b) The transmittance spectra of the absorption filters of thickness 0.8 μm and 3.4 μm. (c) Obtained fluorescent image using the image sensor integrated with the thin-film absorption filter. Fluorescent microspheres (ϕ = 15 μm) were placed directly onto the image sensor and illuminated by excitation light using a blue LED. Representative fluorescent intensity profile along x-pixels was shown at the upper-right corner. The experimental data (dots) were fitted by a Gaussian function (line).

3.2 Evaluation of epi-illumination method

The requirements in regard to epi-illumination of brain tissue for fluorescence imaging are (i) delivery of sufficient excitation light intensity and (ii) uniformity of excitation light at the imaging area. Epi-illumination of biological tissues results in a light intensity gradient in biological tissues because of interactions such as scattering and absorption between light and tissues. Therefore, to evaluate the spatial changes in the excitation light intensity, light propagation in the brain tissue was investigated experimentally and numerically. Figure 5(a) shows the light intensity distribution of excitation light calculated by numerical simulation.

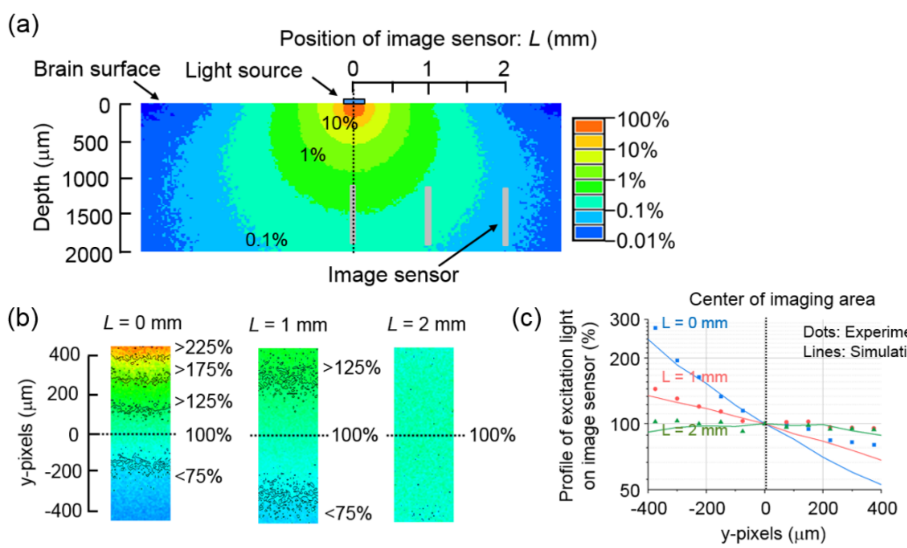

Fig. 5. Numerical analysis of the intensity distribution of excitation light in brain tissues. (a) Cross-sectional image of excitation light intensity in brain tissues. Contours represent the surfaces where the light intensity drops to 10%, 1%, and 0.1%. (b) Normalized excitation light intensity on the surface of the image sensor at various positions (L = 0, 1, and 2 mm). (c) Experimentally measured light intensity profiles (dots) and computationally calculated light intensity profiles (lines) at various positions (L = 0, 1, and 2 mm) as a function of y-pixels.

#235764 - $15.00 USD Received 6 Mar 2015; accepted 16 Mar 2015; published 2 Apr 2015

Light intensity at 1–2 mm depth in the brain tissue was reduced in the range 0.04–0.7%. Apart from the aforementioned scattering and absorption effects, light intensity also decreases as a result of the symmetrical spreading of light from the light-emitting face of the LED. Similar results of symmetrical light propagation in brain tissue were reported in the previous literature [26].

Uneven illumination of the sample will introduce undesired contrast in a fluorescent image. Thus, the excitation light intensity in the imaging area should be uniform to obtain acceptable *in vivo* fluorescent images. Figure 5(b) shows the distribution of the normalized excitation light intensity at the surface of the image sensor for various positions in the brain tissue (position of image sensor: L = 0, 1, and 2 mm). Numerically calculated and experimentally obtained excitation light intensity profiles as a function of y-pixels (μm) are plotted in Fig. 5(c). The light intensity gradients between the excitation light intensity at the top pixels (y-pixel = 400 μm) and the center pixels (y-pixel = 0 μm) were 175% and 44% with the image sensors at L = 0 and 1 mm, respectively. Relatively large and moderate gradients of excitation light intensity on the image sensor remained. In contrast, the light intensity gradient of the image sensors at L = 2 mm was less than 10%. Thus, the relative position of L = 2 mm offers uniform illumination of excitation light on the imaging area.

3.3 Fluorescence imaging in deep brain tissue

Figure 6(a) shows epi-illumination of brain tissue using an LED. Excitation light was delivered from a light source at the brain surface. Light scattering in the brain tissue was observed. Figure 6(b) shows the fluorescent images that were obtained by the image sensor at each positions (L = 0, 1, and 2 mm). Using the epi-illumination method, fluorescent microspheres mimicking fluorescent cells on the image sensor were clearly observed in deep brain tissue (1–2 mm in depth). The image obtained by the image sensor directly under the light source (L = 0 mm) showed high intensity distribution, and the fluorescent intensity was saturated in the top sensor area. Figure 6(c) plots the ratio of the fluorescent intensity of

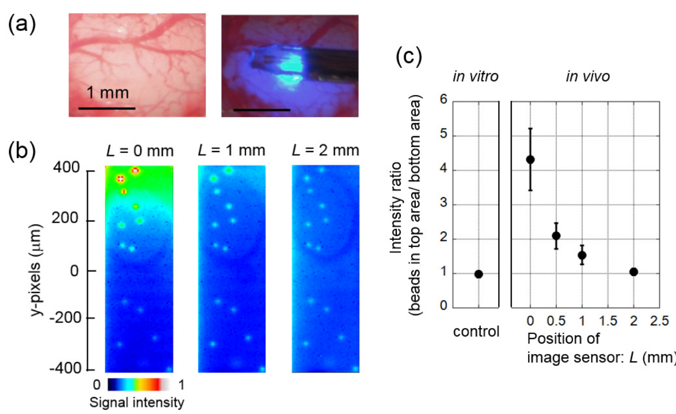

Fig. 6. Fluorescence imaging in deep brain tissues using the implantable semiconductor device. (a) Photographs of the exposed brain surface of a mouse and illuminated brain surface using an LED. (b) Obtained images of fluorescent microspheres (ϕ = 15 μm) in deep brain tissue (1–2 mm in depth) by implanted image sensors at various positions (L = 0, 1, and 2 mm). Saturation of fluorescent signal in the top sensor area (y-pixel > 300 μm) was observed with the image sensor at L = 0 mm. Elliptical shadowing in the images was considered to be an artifact caused by a silicone rubber sheet used to attach microspheres on the device. (c) The ratio of the fluorescent intensity of microspheres in the top sensor area (y-pixel > 300 μm) and bottom sensor area (y-pixel < –300 μm). The intensity ratio of the image sensor at L = 2 mm was at the same level as that of a control image obtained under uniform illumination *in vitro*. Error bars show the standard deviations.

microspheres in the top sensor area (y-pixel > 300 µm) and the bottom sensor area (y-pixel < –300 µm). The intensity ratio were 4.1 ± 0.7, 2.0 ± 0.3, 1.5 ± 0.2, and 1.0 ± 0.1 at L = 0, 0.5, 1, and 2 mm, respectively. The image obtained at L = 0 mm showed a relatively high value of the intensity ratio and the intensity ratio decreased as in proportion to L. The image at L = 2 mm showed the same level of the intensity ratio as the image obtained under uniform illumination condition *in vitro* as a control. This indicates that the relative position of L = 2 mm between the light source and the image sensor achieved uniformity of excitation light in the imaging area for intravital fluorescence imaging.

3.4 Fluorescence imaging of fluorescent substance embedded in brain tissue

Figure 7(a) shows a representative fluorescence image of the microsphere embedded in the brain-tissue slice. Light absorption and scattering in the brain tissue caused signal attenuation and loss of resolution, as shown in Fig. 7(b). Typical signal-to-noise ratios (SNR = fluorescent signal power/ back-ground signal power) of the fluorescence imaging of the microspheres that were located directly on the sensor surface and embedded in the brain tissue, were 15.3 ± 1.7 and 1.9 ± 0.3, respectively. The FWHM values of each signals obtained from the microspheres were 22.3 ± 0.5 µm and 50.3 ± 6.4 µm, respectively. Although light absorption and scattering in the brain tissue caused signal attenuation and loss of resolution, fluorescent signals from fluorescent substances embedded in the brain tissue can be detected by the image sensor. Therefore, the imaging platform is applicable to monitor the activity of neural cells as a group or region, without dividing single cells, and to monitor biochemical reactions in the brain, even at a distance from the sensor. Finally, an implantable semiconductor imaging device was applied to the fluorescence imaging of the brain blood vessels in the brain of a living mouse. Figure 7(c) shows the fluorescence signal change (ΔF) before and after the injection of quantum dots. We obtained fluorescence images of the brain's blood vessels embedded in the brain tissue at the surface.

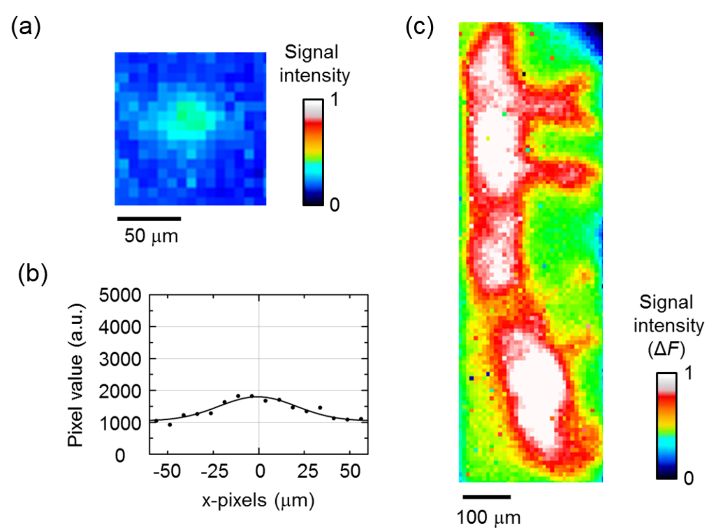

Fig. 7. Fluorescence imaging of fluorescent substances embedded in brain tissues obtained using the implantable semiconductor device. (a) Obtained images of fluorescent microspheres (ϕ = 15 µm) embedded in a 50-µm-thick brain tissue slice. (b) Representative fluorescent intensity profile along x-pixels of the microsphere embedded in brain tissue slice. The experimental data (dots) were fitted by a Gaussian function (line). (c) Fluorescence signal change of blood vessels embedded in the brain tissue of a living mouse that was labeled with quantum dots.

4. Discussion

Optical simulation with interaction between photons and biological tissues has advanced greatly and is intensively used in the biomedical fields, particularly in photodynamic therapy (PDT) [27,28] and optogenetics [6,26]. One of the challenges in the fields is light delivery, because scattering and absorption cause optical attenuation in the living body. To achieve optimal conditions for light delivery, optical simulation is highly useful for the prediction of optical propagation in biological tissues [23,29,30]. Our study using optical simulation demonstrated its utility in intravital imaging. Optical simulation can be used as a powerful tool to solve specific issues in intravital imaging, such as edge blurring and resolution loss of the image due to light absorption and scattering in biological tissue.

The sample illumination technique has been intensively investigated to obtain microscopic images with fidelity. Uneven (non-uniform) illumination reduces the signal range and the quality of optical images and also makes it difficult to remove the back ground and analyze spatial signal changes. For uniform illumination, proper settings for Koehler illumination [31] are a critical in the use of tabletop-type microscopes. In addition, optical diffusers can be used to create uniform illumination. Optical diffusers are broadly classified into two types: surface-relief-type and volumetric type [32]. Surface-relief type optical diffusers can scatter light employing the microstructures on the surface [33,34], whereas volumetric-type optical diffusers can scatter light employing the scattering media [35,36]. From the stand-point of creating uniform illumination, it is noteworthy that our epi-illumination method utilizes biological tissues as a volumetric-type optical diffuser.

Next, we discuss the SNR of the fluorescence imaging using the implantable semiconductor device. The leakage of the excitation light increased the back-ground noise and was primarily responsible for the degradation of the SNR of fluorescence imaging using this imaging platform. LEDs usually emit light with wide band widths, and the broad tail in the long wavelength region often overlaps with the transparent wavelength of the absorption filter, thus cause excitation light leakage. Therefore, to prevent excitation light leakage, we used a blue LED in this imaging platform. The use of coherent light sources, such as laser diodes, which have narrow band widths, will enable us to prevent excitation light leakage. Speckle noise may be detected while using coherent light sources.

The small size of the device contributes to minimizing the invasiveness, and the brain-tissue damage of the device implantation was confirmed to be negligible during the analysis of the brain function [37]. Heat damage and optical damage from the LED illumination were also considered to be negligible, because the LED worked in the linear output region without any increase in temperature, and the light intensity was several tens to several hundreds of times lower than the safety threshold (~4 W cm^{-2}) for tissue [38].

Moreover, intravital fluorescence imaging using quantum dots has been demonstrated to have promising use in biological studies. In this imaging platform, quantum dots that have a large stokes shift (> 100 nm) [39] are preferred as fluorescent probes when compared to organic probes, which have a short stokes shift (20-50 nm). In addition, the labeling technique using quantum dots has a wide range of intravital imaging applications in biological studies [40,41]. Intravital imaging using implantable image sensors enables us to obtain the long-term time-series images of blood vessels in living animals, and it is therefore expected to be useful, especially, in studies of the angiogenesis of tumors in cancer research [42] and the vascularization of engineered tissues in regenerative medicine [43].

5. Conclusions

In conclusion, we developed an intravital fluorescence imaging method using a combination of an implantable semiconductor device and epi-illumination of biological tissue. The sub-millimeter-sized devices, which were designed to be implanted into a certain part of mouse brain, showed sufficient performance for fluorescence imaging, such as optical-filter transmittance: $T < 10^{-5}$ (at 470 nm) for rejection of excitation light and FWHM = 22.3 ± 0.46 μm (ϕ = 15 μm) for resolution of the image. Then, we investigated the epi-illumination method and optical simulations showed the excitation light distribution in the brain tissue. The optimal geometric position of the light source and the image sensor was predicted in the simulation and uniform illumination was successfully achieved. Finally, intravital fluorescence imaging was demonstrated in deep brain tissue (1–2 mm in depth). In addition, we also demonstrated the intravital fluorescence imaging of blood vessels labeled with quantum dots at the brain surface. The implantable semiconductor imaging device based on CMOS technology, which was compact and mass-producible, is expected to be a powerful tool in brain research.

Acknowledgments

The authors would like to thank S. Shiosaka (NAIST) for valuable discussions. This research was supported by Project for Promotion of Researches toward Creation of Humanophilic Science and Technology and Grants-in-Aid for Scientific Research (A) (#26249051) from the Ministry of Education, Culture, Sports, Science and Technology (MEXT) of Japan, and VLSI Design and Education Center (VDEC), The University of Tokyo, in collaboration with Cadence Corporation and Mentor Graphics Corporation.

Additional information

Competing financial interests: The authors declare no competing financial interests.